



Trimetallic composite nanofibers for antibacterial and photocatalytic dye degradation of mixed dye water

Ashish Gupta¹ · Nayna Khosla¹ · V. Govindasamy² · Amit Saini¹ · K. Annapurna² · S. R. Dhakate¹

Received: 3 June 2020 / Accepted: 13 August 2020 / Published online: 25 August 2020
© King Abdulaziz City for Science and Technology 2020

Abstract

Membrane technology is an advanced approach to making a healthier and cleaner environment. Using such catalytic membrane technology to get clean, usable water by removal of dye impurities as well as pathogenic microbes is the main goal behind the research work. Here, we present the synthesis and efficacy study of polymethyl methacrylate (PMMA)-based Ag/ZnO/TiO₂ trimetallic bifunctional nanofibers with antibacterial and photocatalytic activity. The nanofibers have been proven to be effective for the degradation of methylene blue (MB 93.4%), rhodamine B (Rh 34.6%), auramine-O (Au 65.0%) and fuchsin basic (FB 69.8%) dyes individually within 90 min in daylight. The study is further extended in abating a mixture of these dyes from contaminated water using composite nanofibers. Also, in the case of a mixture of these dyes (3 ppm each), nanofibers show dye degradation efficiency (DDE) of 90.9% (MB), 62.4% (Au) and 90.3% (FB and Rh) in 60 min. The role of Ag nanoparticles with a synergic photocatalytic effect on ZnO and TiO₂ is also demonstrated. Also, PMMA/ZnO/TiO₂ composite fiber membrane in synergy with silver particles shows better antibacterial activity against Gram-negative bacteria *E. coli*, making PMMA/Ag/ZnO/TiO₂ fibers a promising candidate in water purification.

Keywords Nanofibers · Membrane · Photocatalysis · Antibacterial · Dye mixture

Introduction

With an increase in industrialization, population and climate change, water pollution has been increasing day by day. According to a survey (Malwal and Gopinath 2017; Thavasi et al. 2008), freshwater shortage and crisis may increase to 50% by 2025 and 75% by 2075 globally. Different pollutants such as dyes, fluoride and heavy metal ions contaminate freshwater, and are hazardous to human beings (Sharma et al. 2014). The polluted water bodies often act as a host breeding ground for bacteria (such as *E. coli*) and pathogens. Statistical data show that about 20% of water pollution is due

to various dyes released in the flowing water (Chavan 2001). Owing to the need of the hour, different water treatment and purification methods such as ozonation (Piaskowski et al. 2018), flocculation (Guo et al. 2018), floatation, and electrolysis (Mokif 2019) have been often utilized for dye removal (Galindo et al. 2001). However, due to the high stability of the dyes and aromatic nature of the dye molecules, biological treatment methods are ineffective for degradation (Arslan and Balcioğlu 1999; Correia et al. 1994; Moore et al. 1989; Patil and Shinde 1988). The other traditional physical removal techniques such as adsorption on activated carbon (Aboua et al. 2015), ultrafiltration (Bouazizi et al. 2017; Hidalgo et al. 2018), reverse osmosis (Sahinkaya et al. 2018), and coagulation by chemical agents (Butler et al. 2017) only transfer the organic compounds from water to another phase, thus causing secondary pollution resulting in enhanced post-treatment cost of solid waste management (Cooper 1993; Galindo et al. 2001). Several metal oxide semiconductor materials are now being used for their excellent photocatalytic activity such as ZnO, TiO₂, and CeO₂ (Younis et al. 2018), and metal sulfides (Shamraiz et al. 2016) such as MnS (Hussain et al. 2019a) and CoS (Hussain et al. 2019b) in abating harmful dyes from drinking water.

Electronic supplementary material The online version of this article (<https://doi.org/10.1007/s13204-020-01540-6>) contains supplementary material, which is available to authorized users.

✉ S. R. Dhakate
dhakate@nplindia.org

¹ Advanced Carbon Products and Metrology, CSIR-National Physical Laboratory, Dr. K.S. Krishnan Marg, New Delhi 110012, India

² Division of Microbiology, Indian Agricultural Research Institute, Pusa Campus, New Delhi 110012, India

These photocatalytic agents can overcome the problem of secondary waste; however, these are difficult to remove from water post-purification due to being in powder form.

To overcome the difficulty of removal of photocatalytic agents post-water treatment, photocatalytic membrane reactors have been developed using various membrane techniques (Molinari et al. 2000, 2001, 2002a, b; Sopajaree et al. 1999a, b), but these processes are of high cost. On the other hand, electrospinning is a simple technique that yields nanofibers with excellent physicochemical properties (Gupta et al. 2019; Moheman et al. 2016; Sharma et al. 2014), which are beneficial for the photocatalytic reaction due to higher mesoporosity and specific surface area. This enhances solar light absorption with visible light sensitivity, longer lifetimes of photogenerated charge carriers and long nanofibrous structure for efficient charge transfer and recovery. Enhancement of photocatalytic activity has been an active area of research since a very long time and it is reported that composite semiconductor materials have higher photocatalytic activity than a single metal oxide semiconductor (Pei and Leung 2013; Sehar et al. 2019). Therefore, bi-complex nanofibers produced by electrospinning have proven to be a promising water treatment material (Yar et al. 2017). Transition metal oxides such as ZnO and TiO₂ are used as active photocatalysts due to their electronic structure with a bandgap energy ~ 3 eV and, thus, can easily generate charge carriers when stimulated with the light of energy lying in the near-visible region. Hence, their performance has been observed even in suitable sunlight (Gupta et al. 2015a). The development of combined photocatalysts and use of solar radiations (cheap, renewable source $\lambda > 300$ nm) are sensible for the reduction of water pollution caused by dye compounds because of the mild conditions required and their efficiency in mineralization (Augugliaro et al. 2002; Sakthivel et al. 2003; Stylidi et al. 2003; Zhang 1996). These catalysts are non-toxic, inexpensive and possess relatively high chemical stability (Pirkanniemi and Sillanpää 2002). However, these oxide materials suffer from a high recombination rate of photogenerated carriers. Recent studies have shown that combining oxides with metal particles such as silver (Ag) (Bian et al. 2020), gadolinium (Gd) (Younis et al. 2016), or indium (In) (Younis et al. 2018) can lower the recombination rate and enhance the photocatalytic activity. Silver (Ag) is also well known to possess antibacterial properties (Nigussie et al. 2018) and it can act as a suitable scavenger during photocatalysis, thereby preventing further recombination and enhancing the photocatalytic efficiency (Fageria et al. 2014). In literature single or bi-metal oxide polymer composite nanofibers are reported for photocatalytic and antibacterial action. It is reported that TiO₂-ZnO nanocomposites can have better and enhanced photocatalytic and antibacterial performance as compared to individual (Di Mauro et al. 2017; Im et al. 2008; Pant et al. 2013; Yar et al. 2017; Zhao et al. 2017).

Polymers are low-cost materials and immobilization of photocatalytic agents over or inside polymer nanofibers is an effective low-cost method. Polymethyl methacrylate (PMMA) is a lightweight, low density, optically transparent and water-insoluble polymer (Kumar et al. 2020) and it is used for immobilization of catalysts as well (Kumar et al. 2013). Also, being hydrophobic, PMMA interacts with aromatic dye molecules and increases dye removal capacity from water (Di Mauro et al. 2017). Also, the immobilization of active particles in the polymer matrix eliminates the difficulty in the separation of materials after dye degradation.

The key importance of the present investigation is to evaluate the dual application of electrospun nanofiber membrane for removal of dyes (a mixture of dyes) from contaminated water and antibacterial activity. Numerous studies are available on the removal of individual dyes (Phan and Kim 2020; Zhao et al. 2017); as one application, however, recently Hussain et al., demonstrated metal sulfides-based materials for purification of water as well as anode material for batteries (Hussain et al. 2019a, b). To our best knowledge, there is no study available in the literature on the removal of dye mixture and antibacterial activities by using nanofibers.

Therefore in the present investigation, the hybrid electrospun polymer nanofiber membrane has been developed for dual applications. The PMMA-based electrospun nanofibers encapsulated by tri-metal nanoparticles (Ag/ZnO/TiO₂) have been synthesized and these trimetallic nanofiber membranes are characterized by different techniques and studied for both dye degradation and antibacterial activity in the presence of sunlight. The dyes utilized in the present research work are methylene blue (MB), rhodamine B (Rh), auramine-O (Au) and fuchsin basic (FB). The efficiency study of nanofibers in abating these dyes individually as well as their mixture solution in the same and different concentrations is carried out.

Experimental

Materials

PMMA (MW ~ 120,000 by GPC), TiO₂ (99% assay) and silver nitrate (AgNO₃) from Rankem and Sigma-Aldrich, respectively; zinc acetate (assay: 99.5%) from CDH, New Delhi; *N, N* dimethyl formamide (DMF) of assay 99.0% from Thomas Baker; ethanol from Changshu Hong sheng Fine Chemical Co Ltd. were procured and used without further purification. Nutrient agar powder was procured from HiMedia, India.

Synthesis of ZnO nanoparticles

ZnO nanoparticles were synthesized by a simple sol-gel method as described elsewhere (Vanaja et al. 2016). The

0.2 M zinc acetate solution was prepared in 50 ml of deionized (DI) water by stirring at 80 °C and marked as solution I. The 3 M NaOH solution was also prepared separately in 50 ml DI water termed as solution II. Solution II was added dropwise to the solution I with constant stirring. Once both the solutions were mixed well, a gel formation was observed. Afterward, the obtained gel was kept for aging for 4–5 h and then filtered out. The residual gel obtained on filter paper was washed with DI water until the filtrate attained a pH of 7. Finally, the residue was dried in an oven at 80 °C for 6 h and later heat treated at temperature 700 °C in a quartz furnace at a ramp rate of 5 °C/min for 3 h to get ZnO nanoparticles.

Synthesis of TiO₂ nanoparticles

As purchased, TiO₂ particles were heat treated at temperature 700 °C for 3 h in a quartz furnace in air atmosphere to remove any volatiles and moisture.

Synthesis of silver nanoparticles

Silver nanoparticles were synthesized by the in situ solvent reduction process (Pastoriza-Santos and Liz-Marzán 2009) with some modification. In brief, 7 mM silver nitrate along with 20 mM of polyvinylpyrrolidone (PVP) solution was added to 100 ml of DMF and the solution was kept on a magnetic stirrer (IKA C-MAG HS7) at room temperature for 24 h with 2 h UV light exposure. Gradually, the solution turned yellow color after aging. The color change of the solution into yellow signifies the formation of silver nanoparticles (Chaudhary et al. 2014).

Synthesis of PMMA/ZnO/TiO₂ and PMMA/Ag/ZnO/TiO₂ nanofibers

For the synthesis of PMMA/ZnO/TiO₂ nanofibers, 20% w/w of ZnO and TiO₂ particles (1:1) w.r.t. polymer were added in 8.2 g of DMF and kept in an ultrasonication bath for 2 h for dispersion. The 1.8 g of PMMA polymer was then added to the solution and it was kept for magnetic stirring for 6 h for uniform dispersion. Similarly, for preparing PMMA/Ag/ZnO/TiO₂ fibers, 20% w/w of ZnO and TiO₂ particles (1:1) were dispersed in DMF solvent containing Ag nanoparticles using ultrasonication. Afterward, the PMMA polymer was added 1.8 g as in the above case of PMMA Ag/ZnO/TiO₂ and stirred well to make uniform dispersion. The above prepared solution of PMMA/ZnO/TiO₂ and PMMA Ag/ZnO/TiO₂ was filled in the 5 ml syringe with a metallic needle (24 G, 0.5 mm dia) separately and subjected to the electrospinning method at the optimized instrumental parameters, i.e., flow rate 0.4 ml/h, voltage 12 kV, and tip to collector

distance 25 cm. PMMA/ZnO/TiO₂ and PMMA/Ag/ZnO/TiO₂ nanofibers have been designated as PZT and PAZT, respectively, throughout the manuscript. Figure 1 shows the schematics for the synthesis of PAZT nanofibers.

Characterization techniques

The as-synthesized nanoparticles and fibres were characterized for their surface morphology using scanning electron microscope (SEM, VPSEM Zeiss EVO MA-10, Germany equipped with lanthanum hexaboride electron gun) and transmission electron microscope (TEM, Technai G-20 S-TWIN) instruments. Elemental analysis was carried out using EDAX (Oxford Instruments Aztec Energy EDX system with 80 mm X-Max silicon drift detector). Raman study was performed using Renishaw in-Via micro-Raman spectrometer with an excitation source of 514.5 nm ($E = 2.41$ eV). The structural information of composite nanofibers was extracted by X-ray diffraction (XRD, Rigaku diffractometer Cu-K α radiation) analysis. Dye degradation studies were carried out using a UV spectrophotometer (Specord 210 Plus double beam).

Dye solution preparation

To study the photocatalytic removal of dyes using PZT and PAZT nanofibers, methylene blue (MB) dye is taken as a model dye primarily. The concentration of MB dye was prepared at 100 ppm as a standard solution and further diluted to prepare 1, 3, and 5 ppm. The PZT and PAZT

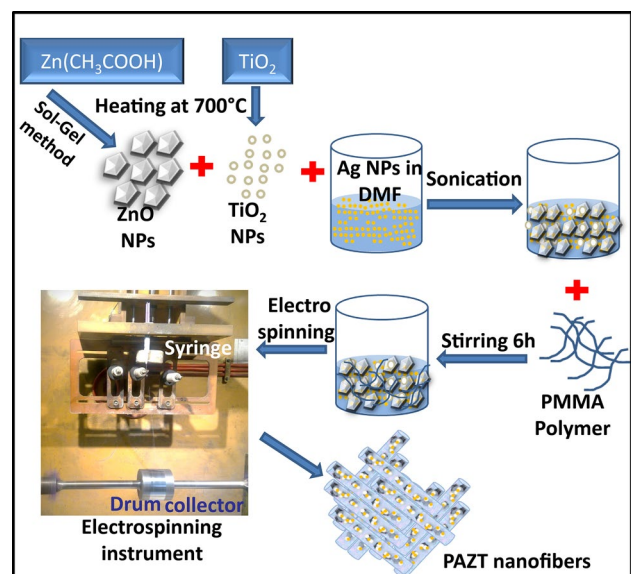


Fig. 1 Schematic of the synthesis process for PAZT nanofibers

nanofibers were tested with 3 ppm concentration of MB dye. 2 mg of the electrospun nanofibers was weighed on a microbalance and added into 10 mL of aqueous dye solution with varying concentration. Then the photocatalytic decolorization of dyes was investigated under the sunlight in the presence/absence of fabricated nanofibers catalysts under irradiation for a given time. The remaining concentration of the dye was evaluated by using the UV–vis spectroscopy from the decrease in corresponding absorbance value as compared to a standard one. The dye degradation efficiency (DDE) is calculated by using the following equation:

$$\text{DDE (\%)} = \frac{A_0 - A}{A_0} \times 100$$

where A_0 is the absorbance for the initial concentration of the dye before irradiation and A is the absorbance for the concentration of the dye after a certain irradiation time.

Further after observing the better efficacy of PAZT over PZT, the PAZT nanofibers were also tested for DDE against MB dye, fuchsin basic (Fb), auramine-*O* (Au) and rhodamine B(Rh) individually. For individual testing, the dye concentration was prepared as 3 ppm for MB, 5 ppm for Au, 1 ppm for each FB and Rh. To study the effect of concentration and time on the photocatalytic action of the PAZT nanofibers were the prime goals. A different set of experiments were carried out on individual dyes as well as a mixture of these dyes.

A mixed dye composed of all four dyes was used in the present work, i.e., MB, Au, FB and Rh. These were mixed in the concentration of 3 ppm each as well as in different concentrations (MB (3 ppm) Au (2 ppm) FB and Rh (1 ppm)) in separate experiments. Self-degradation of dyes was also considered as control under identical conditions for each dye individually as well as in the mixed state.

Zone of inhibition test

Nutrient agar is commonly used to culture various microorganisms in the laboratory to carry out the experiments. The nutrient agar solution was prepared and autoclaved for sterilization and poured into disposable Petri plates under laminar airflow to exclude the microbial contamination which might come during the experiment. 1 ml of Gram-negative *Escherichia coli* (*E. coli* grew on LB broth overnight) strain D#5 α culture was taken and diluted to 10^{-1} . This microbial solution was spread over the solidified agar plates and small pieces of nanofibers were placed over the agar plates. The plates were incubated for 20 h at 37 °C. After 20 h incubation, the antibacterial effect of the PZT and PAZT fibers on *E. coli* strain D#5 α was observed as a

zone of inhibition around the fibers. The zone of inhibition was calculated from the area surrounding the nanofiber pieces using Image J software analysis.

Results and discussion

SEM analysis

The morphology of the synthesized nanoparticles and nanofibers were observed by SEM. Figure 2 shows the SEM images of ZnO nanoparticles, TiO₂ nanoparticles, PZT fibers and PAZT fibers. In Fig. 2a the ZnO nanoparticles are observed with size less than 200 nm measured using Image J software and confirmed from TEM analysis. Most of the ZnO particles have a hexagonal shape, as clearly seen in the magnified image shown in the inset of Fig. 2a. The TiO₂ particles, heat treated at 700 °C and sonicated for 120 min, were observed to be of almost spherical shape (Fig. 2b) and diameter in the range 80–140 nm measured using Image J.

Figure 2c shows the SEM image of PZT fibers having semi-aligned network structure with a diameter in the range 1.1–1.5 μm . The fiber diameter is comparatively more, which may be due to low stretching during electrospinning and deposition of nanoparticles on the surface of fibers. On the other hand, in the case of PAZT nanofibers, the fiber diameter decreases to 0.7–1.2 μm at the same electrospinning processing parameters, due to the presence of Ag nanoparticles in the solution that increases the overall conductivity of the solution (Phan et al. 2020), resulting in more stretching of fibers during electrospinning of solution which attributes to a decrease in the fiber diameter (Fig. 2d). The deposition of particles on the surface of fibers can promote the activity of composite fibers in UV radiation. EDS mapping analysis of PAZT nanofibers shows the presence of Zn, O, Ti, C, and Ag elements in the fibers (supplementary fig. S1).

TEM analysis

Figure 3 shows TEM images for ZnO particles, PZT fibers and PAZT fibers. ZnO particles were sonicated first before preparing a sample for TEM which helps in separating aggregates. Figure 3a shows that ZnO particles are of random size, i.e., 30 nm–200 nm. Figure 3b shows the HRTEM image of the ZnO particle, which shows the parallel fringes. These fringes were further magnified using FFT in Gatan software (inset Fig. 3b) measuring a d -spacing of 0.25 nm (taken from an average of 10 fringes) prominently for the hkl plane (101), which is also confirmed from XRD analysis. Figure 3c shows the TEM image of PZT fibers. The nanoparticles of size 60–170 nm (measured using image J) can be seen clearly on the surface of fibers. The polymer fibers get swelled due to solvent absorption during the sonication

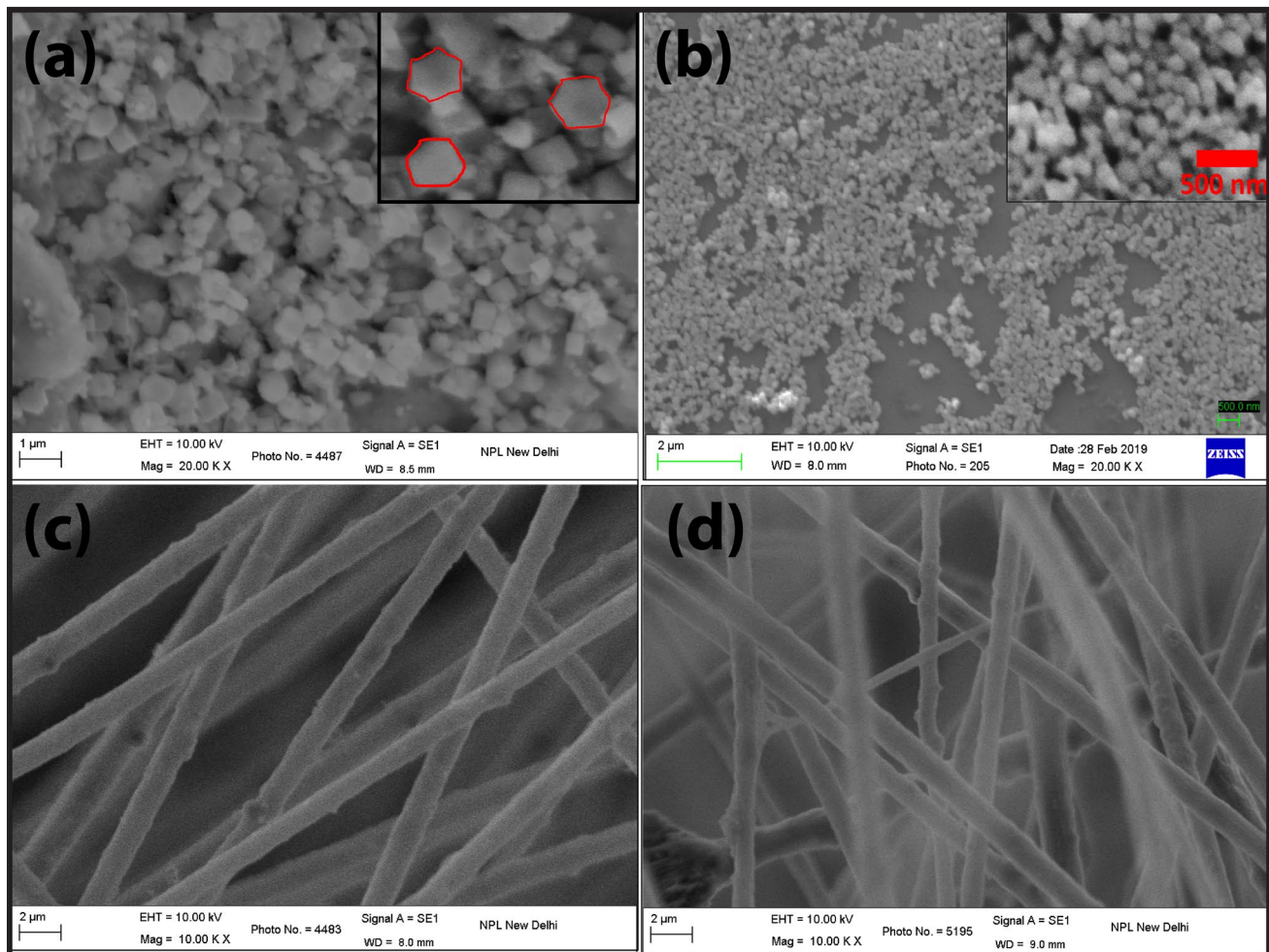


Fig. 2 SEM images of as-synthesized **a** ZnO particles, **b** TiO₂ particles, **c** PZT fibers, **d** PAZT fibers

process and adapted for sample preparation. Similarly, nanoparticles can be seen on the PAZT fibers (Fig. 3d). These nanoparticles may be present inside the fibers or on the surface. However, in a more clear view (inset Fig. 3 (d₁), from contrast change, it seems that these particles have a coating on their surface. It can be assumed that due to polymer coating (size 9–10 nm), a clear planar structure of the particles was not observed.

XRD analysis PZT and PAZT

Figure 4 shows the XRD spectra for ZnO, TiO₂, PZT nanofibers and PAZT nanofibers. Figure 4a shows ZnO is present in hexagonal wurtzite polycrystalline structure form and matches well with JCPDS file 36–1451. It shows the presence of peaks at 2θ values 31.86°, 34.49°, 36.36°, 47.6°, 56.64°, and 69.00°, for hkl value (100), (002), (101), (102), (103) and (112), respectively. Similarly, Fig. 3b shows the XRD curve for TiO₂ particles which matches well with the JCPDS file 21–1272 showing TiO₂ is present in anatase

polycrystalline structure form. More prominent peaks are observed at 2θ values 25.5°, 37.86°, 48.22°, 54.00°, 55.26° and 66.70° for hkl values (101), (004), (200), (105), (211) and (204), respectively. The PMMA nanofibers containing ZnO and TiO₂ (Fig. 3c) were also characterized using XRD and reveal the prominent peaks of TiO₂ for hkl planes (101) and (004) with weak peaks representing ZnO for hkl planes (100) and (002). It can be concluded that TiO₂ may be present on the surface of nanofibers showing higher peak intensity as compared to ZnO, which may be encapsulated inside the fibers. Similar to the above case, in the case of PAZT fibers, the same XRD peaks for ZnO and TiO₂ were observed while peaks for silver are completely hindered due to the high intensity of XRD peaks for substrate aluminum. Aluminum shows XRD peaks at 2θ values 38.45°, 44.71°, 65.09°, and 78.23° for the hkl planes (111), (200), (220) and (311), corresponding to JCPDS no. 89–4037, while Ag also shows peaks nearly at the same positions. This is the reason that the peak for Ag cannot be identified clearly. The XRD peaks at 2θ values 65° and 78° are shown separately

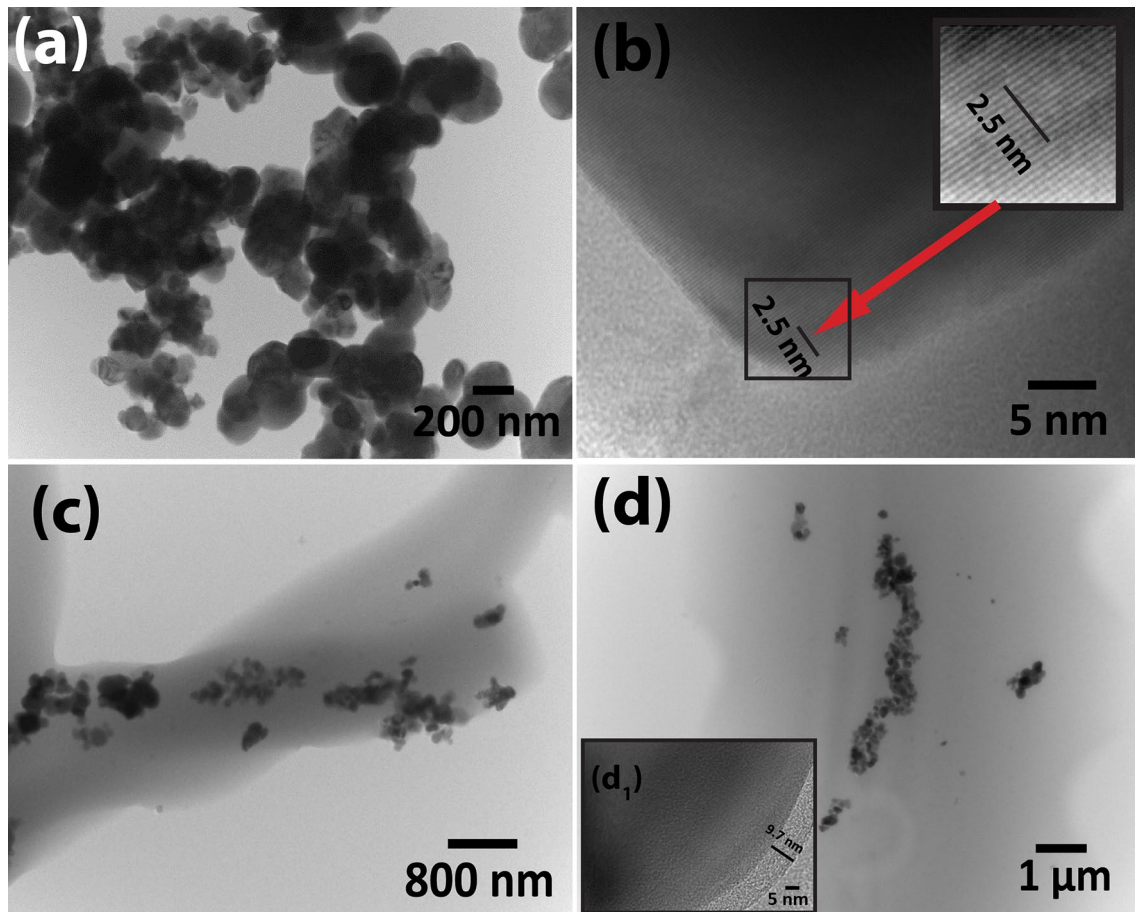


Fig. 3 TEM images of **a** ZnO particles, **b** HRTEM of ZnO particles, **c** PZT fibers and **d** PAZT fibers containing particles

as a magnified image in the inset of Fig. 4c, d. In case of PZT, individual peaks observed at 65.08° and 78.2° (inset of Fig. 4c) can be attributed to aluminum the substrate, while in case of PAZT, duplet peaks are observed (inset of Fig. 4d), i.e., at 65.08° & 65.26° for (220) and 78.2° and 78.44° for (311), representing aluminum and silver (JCPDS 03–0921), respectively.

Raman analysis

Figure 5 shows the Raman spectra for ZnO particles, TiO_2 particles, PZT fibers and PAZT composite fibers. Figure 5a shows the Raman spectrum for as-synthesized ZnO particles. There are eight sets of zone center optical phonons, according to Group theory, out of which two for the transverse optical (TO) phonons, two for longitudinal optical (LO) phonon, two low and high phonon mode as E_2 are Raman active. The peak positioned at 99 cm^{-1} (E_2 low) is dominated by the vibrations of the heavy Zn sub-lattice. The two phonon modes near 438 and 582.85 cm^{-1} could be assigned to E_2 (high) and A_1 (LO), respectively. The peak near 438 cm^{-1} appears due to the presence of oxygen

vibrations (Šćepanović et al. 2010) and confirms the wurtzite phase particularly. The phonon mode at 332 cm^{-1} is a second-order phonon, which generally originates from the zone-boundary phonons of $2E_2$ (low). The Raman spectrum (Fig. 5b) of TiO_2 nanoparticles reveals that four modes, i.e., A_1g , $2B_1g$, and $3E_g$ are Raman active, positioned at peak values 142.5 cm^{-1} (E_g), 196.6 cm^{-1} (E_g), 395.5 cm^{-1} (B_1g), 514.8 cm^{-1} ($A_1g + B_1g$) and 637.5 cm^{-1} (E_g). This confirms that TiO_2 is present in the anatase phase, determined by group analysis D_{4h} ($I_{41/amd}$) (Ma et al. 1998).

In the case of PZT nanofibers, the Raman graph (Fig. 5c) shows the characteristic peak of TiO_2 at $143(E_g)$, $395(B_1g)$, $519(A_1g + B_1g)$ and $639 \text{ cm}^{-1}(E_g)$ (Zhang et al. 2000). A peak appearing near 2951 cm^{-1} is characteristic of the PMMA polymer (Xia et al. 2012). However, no separate peak related to ZnO was observed. It may be because ZnO particles are coated by polymer and small TiO_2 particles, making its Raman signal weak enough to observe. Similar to the above case, in the case of PAZT fibers (Fig. 5d), the Raman graph shows the characteristic peak of TiO_2 at $143(E_g)$, $395.5(B_1g)$, $519.1(A_1g + B_1g)$, and $639.3(E_g) \text{ cm}^{-1}$ revealing the presence of anatase TiO_2 particles on

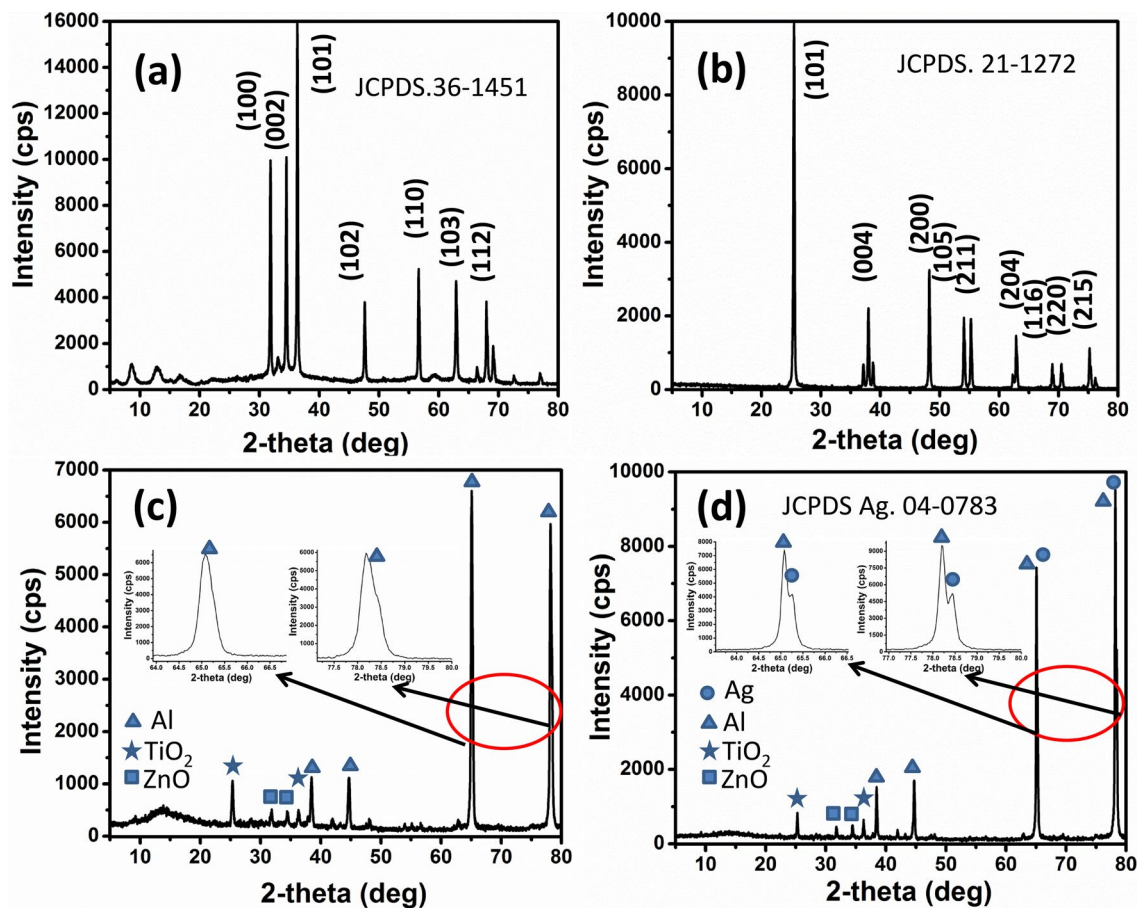


Fig. 4 XRD graph for **a** ZnO particles, **b** TiO₂ particles, **c** PZT and **d** PAZT nanofibers

nanofibers. Pure Ag metal particles are Raman inactive (Ag–Ag bonds), so, no separate peak was observed for Ag particles in [Raman analysis](#) (Michaels et al. 1999), revealing no chemical bonding involving Ag and metal oxides (Zamiri et al. 2014).

PL analysis

Figure 6 shows the PL spectra of PZT and PAZT composite fibers when excited at 360 nm. The PL graph of PZT fibers shows two regions of emission, highest at region 380–450 nm (UV) centered at 404 nm and two weak emissions in the region 482–572 nm (visible) centered at 500 and 560 nm. The peak in the UV region is due to the recombination of electrons from the conduction band with holes in the valence band; such emission is responsible for dye removal activity of these materials. The weak peaks in the visible regions are due to emission from defect sites in composite fibers as well as photocatalytic agents. Although in the case of PAZT a peak with lower intensity (compare to PZT) is observed in the UV region centered at 404 nm, at the same wavelength as PZT; however, lower intensity results are

attributed to low recombination rate (Younis et al. 2016). The recombination rate lowering in PAZT may be due to the presence of silver particles. The decrease in the intensity of emission for PAZT nanofiber with no change in peak position accounts for the interaction between excitons of ZnO/TiO₂ and surface plasmon of Ag nanoparticles (Zheng et al. 2007). Also, in the case of PAZT composite fibers, the peak is not observed in the visible region; this shows the suppression or removal of defect sites that are present in PZT fibers. It may be due to Ag particles that may be trapped in ZnO defect sites and electron transfer takes place between the energy levels of ZnO and Ag metal nanoparticles (Shahi et al. 2020).

UV analysis

The photocatalytic activity of both PZT and PAZT fibers under solar radiation exposure is studied against MB dye using a UV spectrophotometer. Initially, a standard solution of different concentrations of MB was prepared. Figure 7a shows the UV absorption peaks for a standard solution of 5 ppm, 3 ppm and 1 ppm with absorbance value of

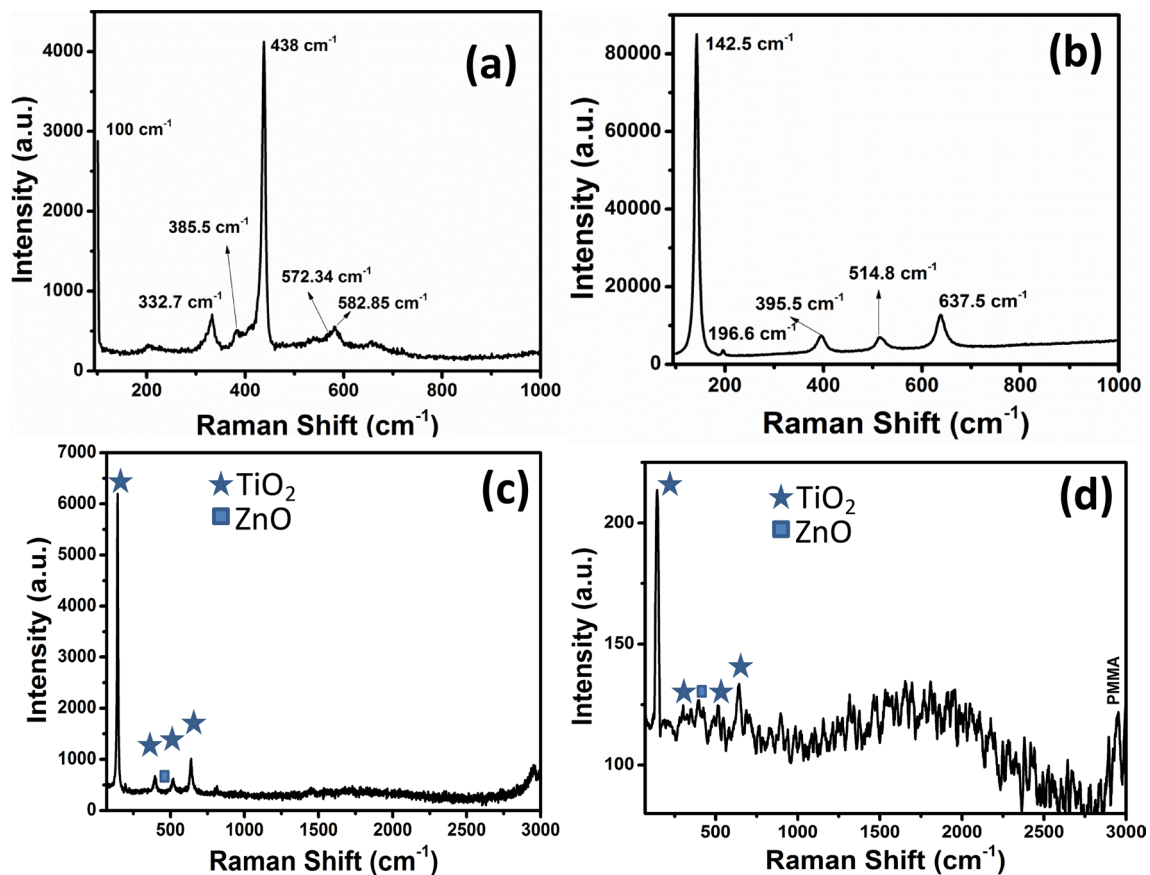


Fig. 5 Raman analysis graphs of (a) ZnO particles, (b) TiO₂ particles, (c) PMMA ZnO/TiO₂ fibers and (d) PMMA Ag/ZnO/TiO₂ fibers

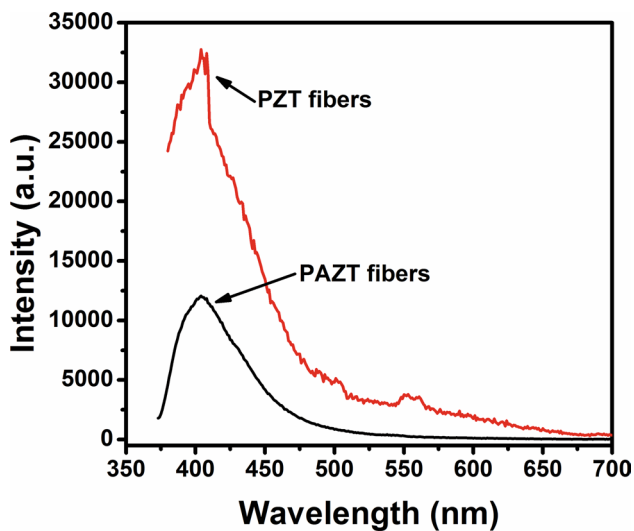


Fig. 6 PL spectrum for PZT and PAZT nanofibers

nearly 0.84, 0.50 and 0.13, respectively. MB dye solution of concentration 3 ppm is used for further photocatalytic studies in solar radiation. Figure 7b shows the change in

absorbance for exposing MB solution containing PZT and PAZT fibers for 20 and 40 min. In the case of PZT fibers, the DDE is 25.7% and 54.2% for 20 and 40 min respectively, while in the case of PAZT fibers, the DDE against MB dye improves and is 42.7 and 71.2% in 20 and 40 min, respectively. The main reason for the improved efficacy is the involvement of Ag, which demonstrated the synergistic effect with ZnO and TiO₂ by surface plasmon resonance (SPR) effect, causing lowering of the recombination rate during exposure to solar radiation (Pant et al. 2013) as observed in PL analysis. In the case of the control (green color curve) sample, the degradation of MB dye in 40 min is observed as only 2.3%.

After observing the better efficacy of PAZT nanofibers in abating MB dye as compared to PZT fibers, the PAZT nanofibers were tested for MB, FB, Au and Rh for different times. Figure 8a shows the photocatalytic activity of MB dye at different time intervals of 30, 60 and 90 min. The DDE for 3 ppm concentration of MB dye is found to be 51.4%, 82.2%, and 93.4% in 30, 60 and 90 min, respectively. The MB dye control exposed to sunlight for 90 min (Fig. 8a) shows dye degradation of 9%. Similarly, for Au dye (5 ppm) (Fig. 8c), PAZT fibers show DDE of 14.1%,

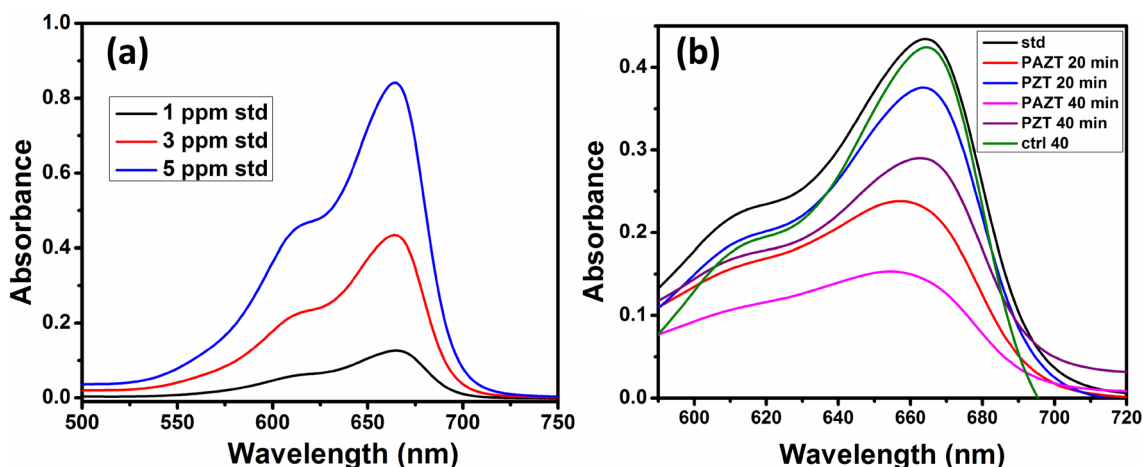


Fig. 7 a Standard curve, b UV plot for photocatalytic activity comparison of PZT and PAZT Nanofibers for MB concentration 3 ppm

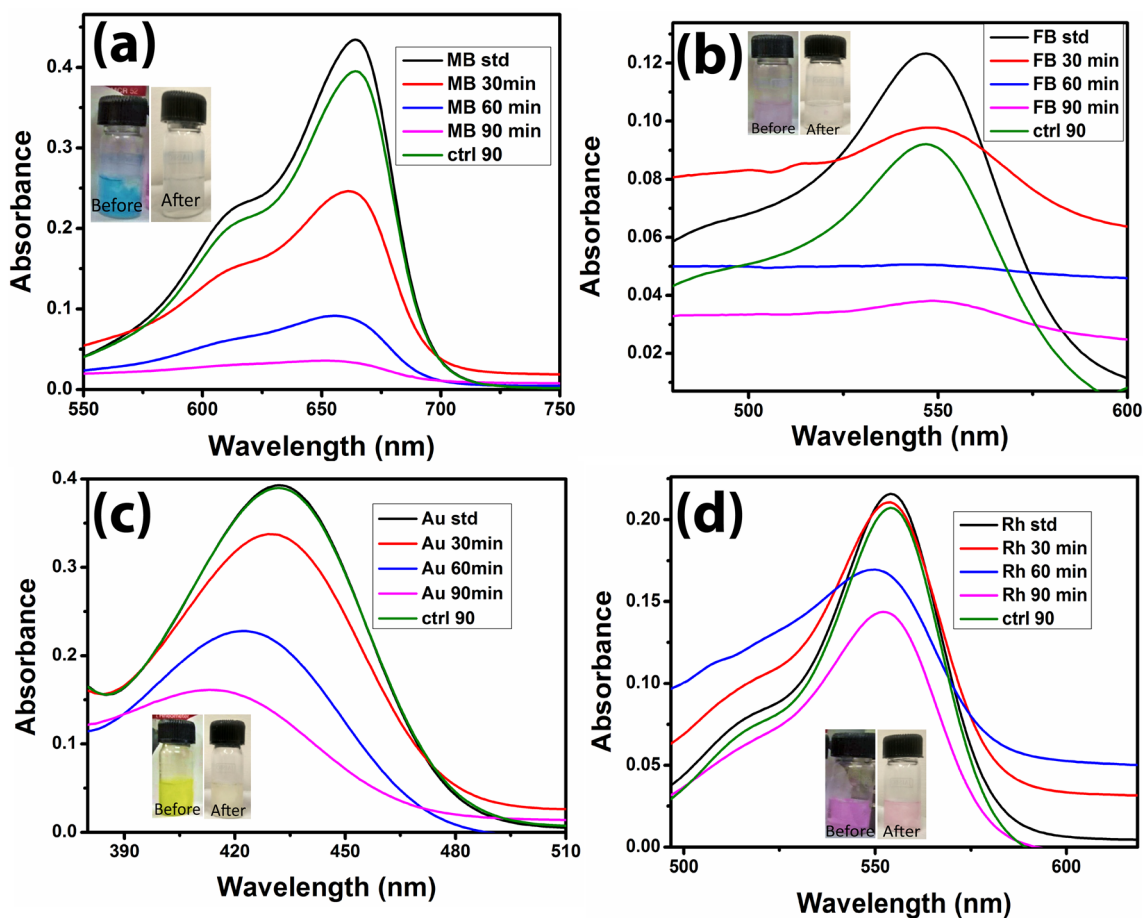


Fig. 8 UV plot of photocatalytic activity of PAZT nanofibers for a MB 3 ppm, b FB 1 ppm, c Au 5 ppm, d Rh 1 ppm (inset: water before and after removal of dye)

44.4% and 65.0% in 30, 60 and 90 min, respectively. The Au dye control sample (5 ppm) shows a degradation of ~1% in sunlight in 90 min.

Further, for FB (1 ppm) (Fig. 8b) and Rh (1 ppm) (Fig. 8d), DDE is 21.0% and 2.6% for 30 min, 59.9% and 23.4% for 60 min, and 69.8% and 34.6% in 90 min,

respectively. This shows that the PAZT fibers are more efficient in abating MB dye followed by FB, AO and Rh. In the case of FB (1 ppm), the control (90 min) shows a degradation of almost 27% and for Rh (1 ppm) 3.9% under sunlight.

Table 1 shows a comparison of photocatalytic activity reported for similar kinds of materials. Although, all the reported materials have shown good performance in abating dye pollutants from water, however, in most cases the dye degradation was carried out for dyes different from our study. These studies also support our assumption of the synergic effect of Ag in combination with ZnO and TiO₂ (Bian et al. 2020; Pant et al. 2013; Zhao et al. 2017). However, most of Ag decorated TiO₂/ZnO composites are in the form of powder

and have limits in easy removal of catalysts from water. As compared to related literature of PMMA/ZnO (20% in 180 min) and PMMA/TiO₂ (70% in 240 min), the time taken by our composite fibers in abating MB dye is less, due to the synergic effect of both ZnO and TiO₂ with similar bandgap and suppressed electron–hole recombination due to presence of Ag particles. The delay in the recombination of charge carriers is also supported by PL analysis of nanofiber materials.

Most of the times, the industrial wastewater consists of these dyes in the mixture form, so, DDE of PAZT fibers against the mixture of these four dyes was also studied. In the first experiment, the concentration of each dye was taken as same (3 ppm) in the mixture. Figure 9a shows the UV

Table 1 Comparison table between literature and present work for individual dyes using nanofibers

Material	Source	Dye	Efficiency	References
PMMA/ZnO nanofibers	UV lamp (8 W, 254 nm)	MB	20% in 180 min	Zhuo et al. (2019)
PMMA/TiO ₂ nanofibers	UV-A	MB	70% in 240 min	Cantarella et al. (2016)
		MO	50% in 240 min	
PMMA/nano-TiO ₂ nanofibers	Sunlight	MO	50% in 5 h	Zhuo et al. (2019)
Rutile-TiO ₂ /PMMA nanofibers	Sun light	MO	30% in 5 h	Liu et al. (2019)
PAN/ZnO nanofibers	UV-A and B	MO	95% in 9 h	Tissera et al. (2018)
PAN/ZnO/TiO ₂	UVC lamp 254 nm	MG	99% in 204 min	Yar et al. (2017)
Ag/TiO ₂ /ZnO nano-flowers	Mercury-vapor lamp	RB	> 80% in 200 min	Pant et al. (2013)
Ag/ZnO /AgO/TiO ₂	Xenon lamp 350 W	RhB	99.3% at 100 min	Bian et al. (2020)
Ag decorated TiO ₂ /ZnO nano-tubes	UV lamp 125 W	MO	96.7% in 35 min for ATZ (100%)	Zhao et al. (2017)
PAN-ZIF-8/Ag/AgCl/ TiO ₂	600 W Xenon lamp $\lambda > 420$ nm	MB	98.02% within 120 min	Zhan et al. (2020)
TiO ₂ /ZnO nanocomposite	300 W halogen lamp	RhB	40% in 60 min	K. S et al. (2017)
PMMA Ag/ZnO/ TiO ₂ nanofibers	Direct sun light	MB, Au, FB, Rh	93.4%, 65%, 69.8%, 34.6% In 90 min	Present work

CV Crystal violet, MB methylene blue, Rh or RhB rhodamine blue, MO methyl orange, FB fuchsin basic, MR methyl red, AR14 acid red14, Au auramine-O, MG malachite green, RB reactive black

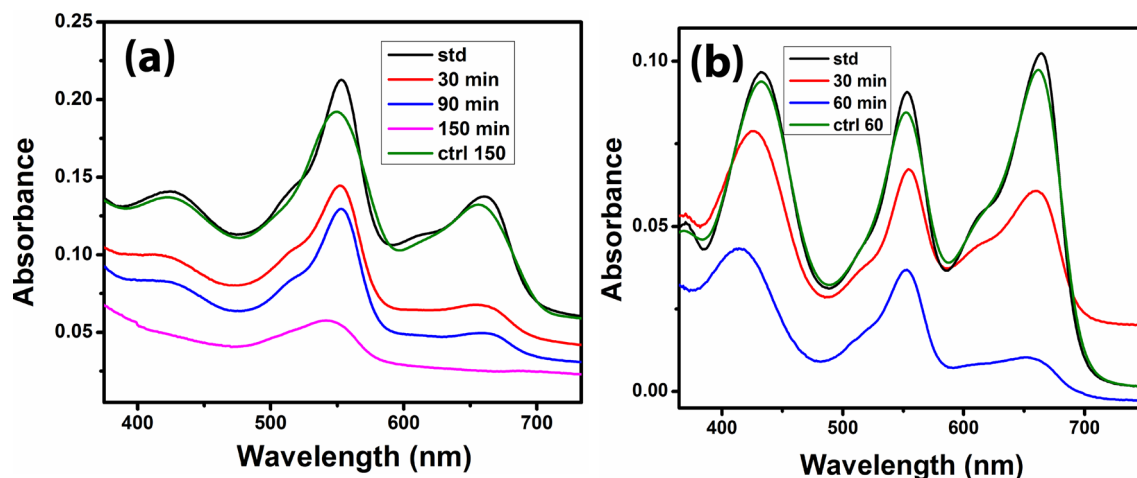


Fig. 9 UV plot of photocatalytic activity of PAZT nanofibers on mix dyes, **a** 3 ppm concentration for each dye, **b** variable concentration (FB: 1 ppm Au: 2 ppm MB: 3 ppm, Rh: 1 ppm)

spectrophotometer analysis of the 3 ppm dye mixture after exposure to PAZT fibers for different time intervals, i.e., 30, 90 and 150 min. The Au and MB dyes show UV peak nearly at two different positions, i.e., 430 and 664 nm, while FB and Rh dye show peak overlapping (peak centers at 553 nm).

The DDE for peak position 430 nm (Au) is found as 30.2%, 41.9%, and 66.0% at 30, 90 and 150 min, respectively. Also, at peak position 664 nm (MB), the dye degradation efficiency was found to be 51.5%, 64.0%, and 81.2% at 30, 90 and 150 min, respectively. The absorption peak at 554 nm (pref. for Rh and FB dye) also showed dye concentration reduction with time and proved that Rh and FB dye have also been degraded by PAZT fibers in solar radiation along with MB and Au dyes simultaneously. The dye degradation efficiency was found to be 32.1%, 39.0% and 74.4% at 30, 90 and 150 min, respectively for peak position 554 nm. The dye degradation without catalyst was found as 2.8% (Au), 10.58% (FB and Rh) and 5.09% (MB) under daylight exposure for 150 min.

The different concentrations of dyes mixture were also prepared containing FB (1 ppm), Au (2 ppm), MB (3 ppm), Rh (1 ppm) and tested in the presence and absence of PAZT fiber in exposure to solar radiations. Similar to the above case, three absorption peak positions were observed for the mixture, i.e., at 430 (Au), 554 (FB and Rh) (Kumar and Kumar 2019; Tokaloğlu et al. 2015) and 664 nm (MB) (Fig. 9b). The control in 60 min shows a dye degradation of 3%, 11.7% and 6% for Au (430 nm), FB and Rh (554 nm),

and MB (664 nm), respectively. The dye degradation efficiency with the catalyst, at peak position 430 nm (Au) is 20.1% and 62.4% at 30 and 60 min, respectively. Also, at peak position 664 nm (MB), the dye degradation efficiency is 41.4% and 90.9% at 30 and 60 min, respectively. The absorption peak at 554 nm (for Rh and FB dye) also shows reduction with time and proved that Rh and FB dye have also been degraded by PAZT fibers in solar radiation along with MB and Au dyes simultaneously. The dye degradation efficiency is found to be 26.0% and 90.3% at 30 and 60 min, respectively, for peak position 554 nm. It is observed that the standard solution absorption differs for the same concentration in case of single dye and mix dyes that may be due to some dye–dye interaction and color change on mixing different color dyes. These results signify the importance of synthesized PAZT fibers that these can be used in water purification by degrading individual as well as a combination of different dyes, i.e., MB, FB, Au and Rh.

Only a few reports (Adamek et al. 2013; Akerdi et al. 2020; Chomkitichai et al. 2019; Gupta et al. 2015b; Xie et al. 2018) are available in the literature on mixed dye removal and most of these reports demonstrate the removal of two dyes that is different from the dyes studied in this work. As can be seen from Table 2, researchers have tried SrTiO₃ (Xie et al. 2018), multi-phase BiVO₄ (Chomkitichai et al. 2019), graphene nanosheets (Gunture et al. 2019), and CoFe₂O₄-RGO (Moitra et al. 2016) photocatalyst for removal of a binary mixture of MB and RhB and/or in

Table 2 Comparison table between literature and present work for dye mixture

Materials	Ex. source	Dye mixture	Dye removal capacity	Refs.
SrTiO ₃ synthesized using sodium carboxymethylcellulose	Mercury lamp 365 nm	RhB–MB binary solution	~ 100% in 180 min	Xie et al. (2018)
Ag ⁺ doped TiO ₂	UV lamp (365 nm)	Crystal Violet and Methyl Red	> 99% on UV irradiation for 90 min	Gupta et al. (2006)
TiO ₂	UV-a lamps	Azodyes effluent from industry	28%(340 nm), 40(430 nm), 58(540 nm), 84 (610 nm)	Adamek et al. (2013)
Multi-phase BiVO ₄	UV lamp (254 nm)	MB and RhB	74% and 21% for catalyst (0.8 g/L) 60 min	Chomkitichai et al. (2019)
GO-TiO ₂ -graphite electrode	9 W UV lamp	MB and AR14	86.74% (MB) and 82.48% (AR14) in 67 min at pH 10	Akerdi et al. (2020)
Graphene nanosheets	Sun light	CV, RhB and MB	~99.9% in 180 min(MB) 225 min (RhB and CV)	Gunture et al. (2019)
CoFe ₂ O ₄ -RGO (25%) catalyst	100 W reading lamp	Methyl orange, Methylene blue, Rhodamine B	99.9% removal in 120 min	Moitra et al. (2016)
PMMA Ag/ZnO/TiO ₂ nanofibers	Sun light	MB, Au, FB, Rh Each 3 ppm	81.2% 66.0% 74.4% in 150 min	Present work
		MB (3 ppm), Au (5 ppm), FB (1 ppm), Rh (1 ppm)	90.9% 62.4% 90.3% in 60 min	Present work

CV crystal violet, MB methylene blue, Rh or RhB rhodamine blue, MO methyl orange, FB fuchsin basic, MR methyl red, AR14 acid red14, Au auramine-O

combination with other dyes. Also, the materials used are in the form of nanomaterials powder as the catalyst. The powder form of the catalyst has the disadvantage of post-degradation removal and also some amount of these may remain in some amount in water, which generates secondary contamination that is harmful to the human body. In our case, Ag/ZnO/TiO₂ nanomaterials are wrapped in the polymer nanofiber matrix, thus making it suitable for real-time application.

The PAZT nanofibers show good photocatalytic activity which may be due to the uniform dispersion of Ag, ZnO and TiO₂ materials in nanofibers, resulting in electron–hole separation to high extent that is enough to perform photocatalytic action for a long time. Also, it is reported that sunlight-induced photocatalysis exhibits higher efficiency and can offer a feasible approach in real-time application (Gunture et al. 2019).

Antibacterial activity

The second goal of the present work is to evaluate the antibacterial performance of synthesized fiber membranes. Antibacterial activity of PAZT and PZT composite fibers membrane was studied by the test of the zone of inhibition using Gram-negative bacterium *E. coli* strain D#5 α . Nanofiber membranes were cut into small pieces and placed under UV exposure for 10 min. Then nanofibers were placed on the surface of the Petri plate and solidified agar medium containing bacterial spread was poured. The plates were lid closed, sealed and kept in an incubator for 24 h at 37 °C. One control sample (without nanofibers sheet) was also kept in an incubator at the same conditions. Figure 10 shows the images of the plates after 24 h incubation. Figure 10(a) shows the image of the control sample. It can be seen that *E. coli* strain D#5 α bacteria have grown uniformly in all directions over the agar medium. In the

case of PZT nanofibers loaded sample, inhibition zones can be seen clearly around the nanofibers (blue circles). The inhibition efficiency for PZT (Fig. 10b) nanofibers sheet was found to be good, but lower in comparison to PAZT (Fig. 10c) nanofibers. The area of the zone of inhibition(%) was calculated using Image J software for each fiber sample shown in Fig. 10. The results have been summarized in Table 2.

As can be seen in Table 3, PZT nanofibers show an inhibition zone area of ~ 172% w.r.t. nanofiber sample which increases to ~ 213% for PAZT nanofibers due to the synergic antibacterial effect of Ag with ZnO and TiO₂. Ag metal particles in contact with ZnO and TiO₂ reduces the bandgap energy by increasing the e⁻–h⁺ charge separation time and thus increases the antibacterial activity as compared to nanofibers containing only ZnO and TiO₂ (Nigussie et al. 2018). The detailed antibacterial mechanism is shown in Fig. 11

Also, it is reported (Yamanaka et al. 2005) that noble metal ions inhibit the enzymes for ATP hydrolysis and expression of ribosomal proteins by hindering DNA replication of bacteria (Fig. 11). The synergic effect of silver nanoparticles with ZnO and TiO₂ is due to its plasmon resonance, where the electrons present on the surface of Ag particles move to the conduction band of ZnO and TiO₂ and get trapped by O₂ molecules to generate O₂, dOOH,

Table 3 Zone of inhibition against *E. coli* bacteria for PZT and PAZT nanofibers

Sample name	Total area of inhibition (%)				Average
	1	2	3	4	
PZT nanofibers	168.0	175.8	171.4	174.2	172.4
PAZT nanofibers	184.4	239.8	214.7	211.5	212.6

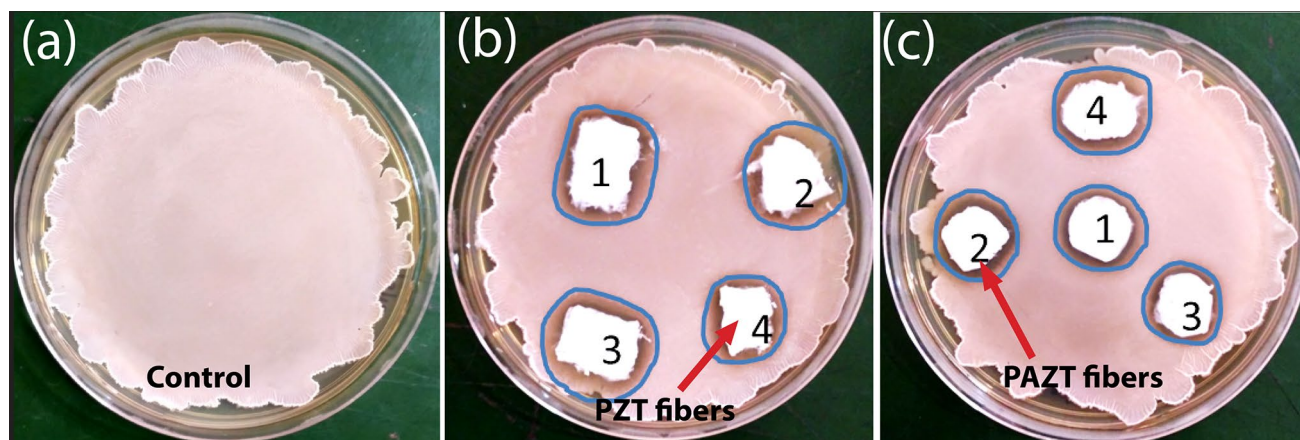
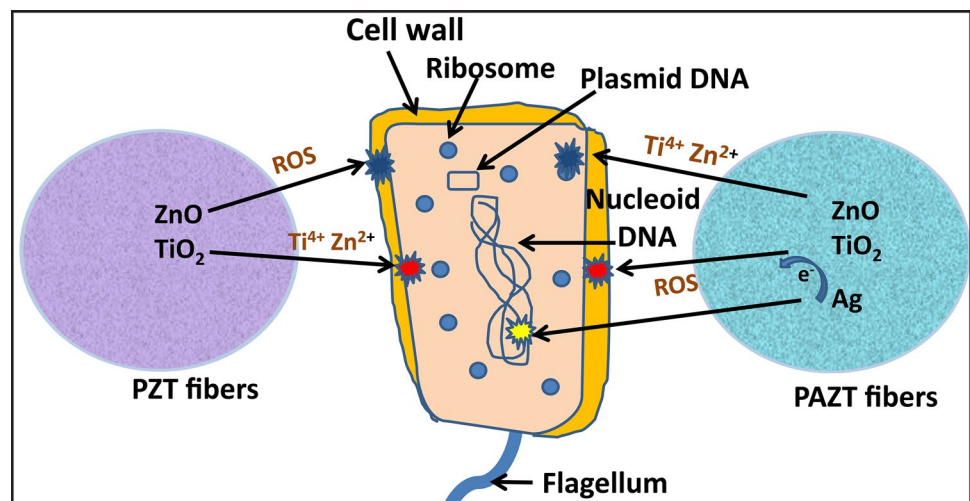


Fig. 10 Antibacterial zone inhibition test for **a** control sample, **b** PZT and **c** PAZT nanofibers

Fig. 11 The proposed mechanism for antibacterial action of PZT and PAZT nanofibers



and dOH (ROS) for complete bacterial destruction (Pant et al. 2013).

Conclusions

Synthesis of tricomponent PMMA composite fiber membrane containing ZnO, TiO₂ and Ag particles was carried out successfully using the electrospinning technique. In the case of PAZT fibers, the diameter decreases due to the addition of Ag conducting particles as a consequence of more elongation at the same processing conditions. The particles are encapsulated inside the fiber and deposited on the surface of fibers. The nanofibers are proven to be effective in abating MB (93.4%), Rh (34.6%), Au (65.0%) and FB (69.8%) dyes individually in 90 min. These nanofibers have demonstrated their utility in abating the mixture of these dyes for 3 ppm concentration of each as well as in different concentrations successfully. The addition of silver in the ZnO/TiO₂ composite further enhances its photocatalytic activity due to the SPR effect of Ag metal ions, lowering the recombination rate. The zone of inhibition against Gram-negative bacteria *E. Coli* is measured as ~172% for PZT fibers, which enhances to ~215% for PAZT fibers due to the synergistic bactericidal effect of Ag with ZnO and TiO₂.

Acknowledgements The authors would like to thank Dr. D. K. Aswal, Director, CSIR-NPL for his kind permission for publication. One of the authors, Dr. Ashish Gupta, thanks the Council of Scientific and Industrial Research (CSIR) for research associateship award (31/01(0499)/2018-EMR-I) to carry out this research work. The authors also like to thank Dr. Jai Tawale and Mr. Dinesh Singh, for SEM and TEM characterization of composite nanofibers.

Compliance with ethical standards

Conflict of interest The authors declare no conflict of interest.

References

- Aboua KN, Yobouet YA, Yao KB, Goné DL, Trokourey A (2015) Investigation of dye adsorption onto activated carbon from the shells of Macoré fruit. *J Environ Manage* 156:10–14
- Adamek E, Baran W, Ziemiańska J, Sobczak A (2013) The comparison of photocatalytic degradation and decolorization processes of dyeing effluents. *Int J Photoenergy* 2013:578191
- Akerdi AG, Bahrami SH, Pajootan E (2020) Modeling and optimization of Photocatalytic Decolorization of binary dye solution using graphite electrode modified with Graphene oxide and TiO₂. *J Environ Health Sci Eng* 18(1):51–62
- Arslan I, Balcioglu IA (1999) Degradation of commercial reactive dyestuffs by heterogenous and homogenous advanced oxidation processes: a comparative study. *Dyes Pigm* 43(2):95–108
- Augugliaro V, Baiocchi C, Prevot AB, García-López E, Loddo V, Malato S, Marcí G, Palmisano L, Pazzi M, Pramauro E (2002) Azo-dyes photocatalytic degradation in aqueous suspension of TiO₂ under solar irradiation. *Chemosphere* 49(10): 1223–1230
- Bian H, Zhang Z, Xu X, Gao Y, Wang T (2020) Photocatalytic activity of Ag/ZnO /AgO/TiO₂ composite. *Physica E* 124:114236
- Bouazizi A, Breida M, Achou B, Ouammou M, Calvo JI, Aaddane A, Younssi SA (2017) Removal of dyes by a new nano-TiO₂ ultrafiltration membrane deposited on low-cost support prepared from natural Moroccan bentonite. *Appl Clay Sci* 149:127–135
- Butler EB, Hung Y-T, Mulamba O (2017) The effects of chemical coagulants on the decolorization of dyes by electrocoagulation using response surface methodology (RSM). *Appl Water Sci* 7(5):2357–2371
- Cantarella M, Sanz R, Buccheri MA, Ruffino F, Rappazzo G, Scalse S, Impellizzeri G, Romano L, Privitera V (2016) Immobilization of nanomaterials in PMMA composites for photocatalytic removal of dyes, phenols and bacteria from water. *J Photochem Photobiol A* 321:1–11
- Chaudhary A, Gupta A, Mathur RB, Dhakate SR (2014) Effective antimicrobial filter from electrospun polyacrylonitrile-silver composite nanofibers membrane for conducive environment. *Adv Mater Lett* 5(10):562–568
- Chavan RB (2001) Indian textile industry-environmental issues. *Indian J Fibre Text Res* 26(1–2):11–21
- Chomkitichai W, Pama J, Jaiyen P, Pano S, Ketwaraporn J, Pookmanee P, Phanichphant S, Jansanthea P (2019) Dye Mixtures

- degradation by multi-phase BiVO₄ Photocatalyst. *Appl Mech Mater* 886:138–145
- Cooper P (1993) Removing colour from dyehouse waste waters—a critical review of technology available. *J Soc Dyers Colour* 109(3):97–100
- Correia VM, Stephenson T, Judd SJ (1994) Characterisation of textile wastewaters—a review. *Environ Technol* 15(10):917–929
- Di Mauro A, Cantarella M, Nicotra G, Pellegrino G, Gulino A, Brundo MV, Privitera V, Impellizzeri G (2017) Novel synthesis of ZnO/PMMA nanocomposites for photocatalytic applications. *Sci Rep* 7:40895
- Divya KS, Xavier MM, Vandana PV, Reethu VN, Mathew S (2017) A quaternary TiO₂/ZnO/RGO/Ag nanocomposite with enhanced visible light photocatalytic performance. *New J Chem* 41(14):6445–6454
- Fageria P, Gangopadhyay S, Pande S (2014) Synthesis of ZnO/Au and ZnO/Ag nanoparticles and their photocatalytic application using UV and visible light. *RSC Adv* 4(48):24962–24972
- Galindo C, Jacques P, Kalt A (2001) Photooxidation of the phenylazonaphthol AO20 on TiO₂: kinetic and mechanistic investigations. *Chemosphere* 45(6–7):997–1005
- Guo K, Gao B, Li R, Wang W, Yue Q, Wang Y (2018) Flocculation performance of lignin-based flocculant during reactive blue dye removal: comparison with commercial flocculants. *Environ Sci Pollut Res* 25(3):2083–2095
- Gupta AK, Pal A, Sahoo C (2006) Photocatalytic degradation of a mixture of Crystal Violet (Basic Violet 3) and Methyl Red dye in aqueous suspensions using Ag⁺ doped TiO₂. *Dyes Pigm* 69(3):224–232
- Gupta A, Nandanwar DV, Dhakate SR (2015a) Electrospun self-assembled ZnO nanofibers structures for photocatalytic activity in natural solar radiations to degrade acid fuchsin dye. *Adv Mater Lett* 6(8):706–710
- Gupta V, Khamparia S, Tyagi I, Jaspal D, Malviya A (2015b) Decolorization of mixture of dyes: a critical review.
- Gupta A, Gurunathan P, Ramesha K, Singh M, Dhakate SR (2019) Effect of heat treatment temperature on energy storage performance of PAN co-MMA based carbon nanofibers as freestanding lithium ion batteries anode. *Energy Storage* 1(6):e89
- Hidalgo AM, Gómez M, Murcia MD, Serrano M, Rodríguez-Schmidt R, Escudero PA (2018) Behaviour of polysulfone ultrafiltration membrane for dyes removal. *Water Sci Technol* 77(7–8):2093–2100
- Hussain W, Malik H, Hussain RA, Hussain H, Green IR, Marwat S, Bahadur A, Iqbal S, Farooq MU, Li H, Badshah A (2019) Synthesis of MnS from single- and multi-source precursors for photocatalytic and battery applications. *J Electron Mater* 48(4):2278–2288
- Hussain W, Malik H, Khan MA, Iqbal MJ, Hussain RA, Shoukat R, Khan Y, Badshah A, Sulaman M, Li H (2019) Comparative study of cobalt sulphides properties for photocatalytic and battery applications. *Semicond Sci Technol* 34(9):095015
- Im JS, Kim MI, Lee Y-S (2008) Preparation of PAN-based electrospun nanofiber webs containing TiO₂ for photocatalytic degradation. *Mater Lett* 62(21–22):3652–3655
- Kumar TKM, P., Kumar S.K., A. (2019) Visible-light-induced degradation of rhodamine B by nanosized Ag₂S–ZnS loaded on cellulose. *Photochem Photobiol Sci* 18(1):148–154
- Kumar P, Gupta A, Dhakate SR, Mathur RB, Nagar S, Gupta VK (2013) Covalent immobilization of xylanase produced from *Bacillus pumilus* SV-85 S on electrospun polymethyl methacrylate nanofiber membrane. *Biotechnol Appl Biochem* 60(2):162–169
- Kumar S, Jain G, Kumar K, Gupta A, Singh BP, Dhakate SR (2020) A facile fabrication of poly(methyl methacrylate)/α-NaYF₄:Eu³⁺ tunable electrospun photoluminescent nanofibers. *Appl Nanosci*. <https://doi.org/10.1007/s13204-020-01499-4>
- Liu J, Zhuo Y, Wang Y, Li Q, Ren X (2019) Preparation and characterization of R-TiO₂/PMMA nanofibers by electrospinning. *Ferroelectrics* 548(1):8–14
- Ma W, Lu Z, Zhang M (1998) Investigation of structural transformations in nanophase titanium dioxide by Raman spectroscopy. *Appl Phys A* 66(6):621–627
- Malwal D, Gopinath P (2017) Efficient adsorption and antibacterial properties of electrospun CuO–ZnO composite nanofibers for water remediation. *J Hazard Mater* 321:611–621
- Michaels AM, Nirmal M, Brus LE (1999) Surface enhanced Raman spectroscopy of individual rhodamine 6G Molecules On Large Ag nanocrystals. *J Am Chem Soc* 121(43):9932–9939
- Moheman A, Alam MS, Gupta A, Dhakate S, Kumar A, Mohammad A (2016) Fabrication of nanofiber stationary phases from chopped polyacrylonitrile co-polymer microfibers for use in ultrathin layer chromatography of amino acids. *RSC Adv* 6(93):90100–90110
- Moitra D, Chandel M, Ghosh BK, Jani RK, Patra MK, Vadera SR, Ghosh NN (2016) A simple ‘in situ’ co-precipitation method for the preparation of multifunctional CoFe₂O₄–reduced graphene oxide nanocomposites: excellent microwave absorber and highly efficient magnetically separable recyclable photocatalyst for dye degradation. *RSC Adv* 6(80):76759–76772
- Mokif LA (2019) Removal methods of synthetic dyes from industrial wastewater: a review. *Mesopot Environ J* 5(1):23–40
- Molinari R, Mungari M, Drioli E, Di Paola A, Loddo V, Palmisano L, Schiavello M (2000) Study on a photocatalytic membrane reactor for water purification. *Catal Today* 55(1–2):71–78
- Molinari R, Grande C, Drioli E, Palmisano L, Schiavello M (2001) Photocatalytic membrane reactors for degradation of organic pollutants in water. *Catal Today* 67(1–3):273–279
- Molinari R, Borgese M, Drioli E, Palmisano L, Schiavello M (2002) Hybrid processes coupling photocatalysis and membranes for degradation of organic pollutants in water. *Catal Today* 75(1–4):77–85
- Molinari R, Palmisano L, Drioli E, Schiavello M (2002) Studies on various reactor configurations for coupling photocatalysis and membrane processes in water purification. *J Membr Sci* 206(1–2):399–415
- Moore AT, Vira A, Fogel S (1989) Biodegradation of trans-1,2-dichloroethylene by methane-utilizing bacteria in an aquifer simulator. *Environ Sci Technol* 23(4):403–406
- Nigussie GY, Tesfamariam GM, Tegegne BM, Weldemichel YA, Gebreab TW, Gebrehiwot DG, Gebremichel GE (2018) Antibacterial activity of Ag-doped TiO₂ and Ag-doped ZnO nanoparticles. *Int J Photoenergy*. <https://doi.org/10.1155/2018/5927485>
- Pant HR, Pant B, Sharma RK, Amarjargal A, Kim HJ, Park CH, Tijing LD, Kim CS (2013) Antibacterial and photocatalytic properties of Ag/TiO₂/ZnO nano-flowers prepared by facile one-pot hydrothermal process. *Ceram Int* 39(2):1503–1510
- Pastoriza-Santos I, Liz-Marzán LM (2009) *N,N*-dimethylformamide as a reaction medium for metal nanoparticle synthesis. *Adv Func Mater* 19(5):679–688
- Patil SS, Shinde VM (1988) Biodegradation studies of aniline and nitrobenzene in aniline plant wastewater by gas chromatography. *Environ Sci Technol* 22(10):1160–1165
- Pei CC, Leung WW-F (2013) Enhanced photocatalytic activity of electrospun TiO₂/ZnO nanofibers with optimal anatase/rutile ratio. *Catal Commun* 37:100–104
- Phan D-N, Kim I-S (2020) Composite nanofibers: recent progress in adsorptive removal and photocatalytic degradation of dyes fiber composites. IntechOpen, London

- Phan D-N, Dorjjugder N, Saito Y, Taguchi G, Ullah A, Kharaghani D, Kim I-S (2020) The synthesis of silver-nanoparticle-anchored electrospun polyacrylonitrile nanofibers and a comparison with as-spun silver/polyacrylonitrile nanocomposite membranes upon antibacterial activity. *Polym Bull* 77(8):4197–4212
- Piaskowski K, Świdarska-Dąbrowska R, Zarzycki PK (2018) Dye removal from water and wastewater using various physical, chemical, and biological processes. *J AOAC Int* 101(5):1371–1384
- Pirkanniemi K, Sillanpää M (2002) Heterogeneous water phase catalysis as an environmental application: a review. *Chemosphere* 48(10):1047–1060
- Sahinkaya E, Sahin A, Yurtsever A, Kitis M (2018) Concentrate minimization and water recovery enhancement using pellet precipitator in a reverse osmosis process treating textile wastewater. *J Environ Manage* 222:420–427
- Sakthivel S, Neppolian B, Shankar M, Arabindoo B, Palanichamy M, Murugesan V (2003) Solar photocatalytic degradation of azo dye: comparison of photocatalytic efficiency of ZnO and TiO₂. *Sol Energy Mater Sol Cells* 77(1):65–82
- Šćepanović M, Grujić-Brojčin M, Vojisavljević K, Bernik S, Srećković T (2010) Raman study of structural disorder in ZnO nanopowders. *J Raman Spectrosc* 41(9):914–921
- Sehar S, Naz I, Perveen I, Ahmed S (2019) Superior dye degradation using SnO₂-ZnO hybrid heterostructure catalysts. *Korean J Chem Eng* 36(1):56–62
- Shahi K, Singh R, Singh J, Aleksandrova M, Singh AK (2020) Synthesis of Ag nanoparticle-decorated ZnO nanorods adopting the low-temperature hydrothermal method. *J Electron Mater* 49(1):637–642
- Shamraiz U, Hussain RA, Badshah A, Raza B, Saba S (2016) Functional metal sulfides and selenides for the removal of hazardous dyes from Water. *J Photochem Photobiol B* 159:33–41
- Sharma R, Singh N, Gupta A, Tiwari S, Tiwari SK, Dhakate SR (2014) Electrospun chitosan-polyvinyl alcohol composite nanofibers loaded with cerium for efficient removal of arsenic from contaminated water. *J Mater Chem A* 2(39):16669–16677
- Singh AG, Bhati A, Khare P, Tripathi KM, Sonkar SK (2019) Soluble graphene nanosheets for the sunlight-induced photodegradation of the mixture of dyes and its environmental assessment. *Sci Rep* 9(1):2522
- Sopajaree K, Qasim S, Basak S, Rajeshwar K (1999a) An integrated flow reactor-membrane filtration system for heterogeneous photocatalysis. Part I: experiments and modelling of a batch-recirculated photoreactor. *J Appl Electrochem* 29(5):533–539
- Sopajaree K, Qasim S, Basak S, Rajeshwar K (1999b) An integrated flow reactor-membrane filtration system for heterogeneous photocatalysis. Part II: experiments on the ultrafiltration unit and combined operation. *J Appl Electrochem* 29(9):1111–1118
- Stylidi M, Kondarides DI, Veyrakis XE (2003) Pathways of solar light-induced photocatalytic degradation of azo dyes in aqueous TiO₂ suspensions. *Appl Catal B* 40(4):271–286
- Thavasi V, Singh G, Ramakrishna S (2008) Electrospun nanofibers in energy and environmental applications. *Energy Environ Sci* 1(2):205–221
- Tissera ND, Wijesena RN, Sandaruwan CS, de Silva RM, de Alwis A, de Silva KMN (2018) Photocatalytic activity of ZnO nanoparticle encapsulated poly(acrylonitrile) nanofibers. *Mater Chem Phys* 204:195–206
- Tokaloğlu Ş, Yavuz E, Aslantaş A, Şahan H, Taşkın F, Patat Ş (2015) Spectrophotometric determination of basic fuchsin from various water samples after vortex assisted solid phase extraction using reduced graphene oxide as an adsorbent. *Spectrochim Acta Part A Mol Biomol Spectrosc* 149:378–384
- Vanaja A, Ramaraju G, Srinivasa Rao K (2016) Role of NaOH concentration on structural, morphological and optical properties of ZnO nanopowders synthesized by solgel process. *Int J Technol Chem Res* 2(2):110–120
- Xia M, Su Z, Zhang S (2012) Raman spectra of bilayer graphene covered with Poly (methyl methacrylate) thin film. *AIP Adv* 2(3):032122
- Xie J, He Y, Wang H, Duan M, Tang J, Wang Y, Chamas M, Wang H (2018) Photocatalytic degradation of binary dyes mixture over SrTiO₃ synthesized using sodium carboxymethylcellulose additive. *Russ J Phys Chem A* 92(4):809–815
- Yamanaka M, Hara K, Kudo J (2005) Bactericidal Actions of a silver ion solution on *Escherichia coli* studied by energy-filtering transmission electron microscopy and proteomic analysis. *Appl Environ Microbiol* 71(11):7589
- Yar A, Haspulat B, Üstün T, Eskizeybek V, Avcı A, Kamyş H, Achour S (2017) Electrospun TiO₂/ZnO/PAN hybrid nanofiber membranes with efficient photocatalytic activity. *RSC Adv* 7(47):29806–29814
- Younis A, Chu D, Kaneti YV, Li S (2016) Tuning the surface oxygen concentration of 111 surrounded ceria nanocrystals for enhanced photocatalytic activities. *Nanoscale* 8(1):378–387
- Younis A, Shirsath SE, Shabbir B, Li S (2018) Controllable dynamics of oxygen vacancies through extrinsic doping for superior catalytic activities. *Nanoscale* 10(39):18576–18585
- Zamiri R, Rebelo A, Zamiri G, Adnani A, Kuashal A, Belsley MS, Ferreira J (2014) Far-infrared optical constants of ZnO and ZnO/Ag nanostructures. *RSC Adv* 4(40):20902–20908
- Zhan Y, Lan J, Shang J, Yang L, Guan X, Li W, Chen S, Qi Y, Lin S (2020) Durable ZIF-8/Ag/AgCl/TiO₂ decorated PAN nanofibers with high visible light photocatalytic and antibacterial activities for degradation of dyes. *J Alloy Compd* 822:153579
- Zhang M (1996) Decolorization and biodegradability of dyeing wastewater treated by a TiO₂-sensitized photo-oxidation process. *Water Sci Technol* 34(9):49–55
- Zhang W, He Y, Zhang M, Yin Z, Chen Q (2000) Raman scattering study on anatase TiO₂ nanocrystals. *J Phys D Appl Phys* 33(8):912
- Zhao S, Cheng Z, Kang L, Li M, Gao Z (2017) The facile preparation of Ag decorated TiO₂/ZnO nanotubes and their potent photocatalytic degradation efficiency. *RSC Adv* 7(79):50064–50071
- Zheng Y, Zheng L, Zhan Y, Lin X, Zheng Q, Wei K (2007) Ag/ZnO heterostructure nanocrystals: synthesis, characterization, and photocatalysis. *Inorg Chem* 46(17):6980–6986
- Zhuo Y, Liu J, Wang Y, Li Q, Xu X, Ren X (2019) Preparation and photocatalytic property of electrospun nano-TiO₂/poly(methylmethacrylate) nanofibres. *Ferroelectrics* 548(1):143–149

Publisher's Note Springer Nature remains neutral with regard to jurisdictional claims in published maps and institutional affiliations